

High-pressure behavior of natural single-crystal epidote and clinozoisite up to 40 GPa

Fei Qin^{1,4} · Xiang Wu¹ · Ying Wang¹ · Dawei Fan² · Shan Qin¹ · Ke Yang³ · Joshua P. Townsend⁴ · Steven D. Jacobsen⁴

Received: 25 February 2016 / Accepted: 13 June 2016 / Published online: 27 June 2016
© Springer-Verlag Berlin Heidelberg 2016

Abstract The comparative compressibility and high-pressure stability of a natural epidote (0.79 Fe-total per formula unit, Fe_{tot} pfu) and clinozoisite (0.40 Fe_{tot} pfu) were investigated by single-crystal X-ray diffraction and Raman spectroscopy. The lattice parameters of both phases exhibit continuous compression behavior up to 30 GPa without evidence of phase transformation. Pressure–volume data for both phases were fitted to a third-order Birch–Murnaghan equation of state with $V_0 = 461.1(1) \text{ \AA}^3$, $K_0 = 115(2) \text{ GPa}$, and $K'_0 = 3.7(2)$ for epidote and $V_0 = 457.8(1) \text{ \AA}^3$, $K_0 = 142(3) \text{ GPa}$, and $K'_0 = 5.2(4)$ for clinozoisite. In both epidote and clinozoisite, the *b*-axis is the stiffest direction, and the ratios of axial compressibility are 1.19:1.00:1.15 for epidote and 1.82:1.00:1.19 for clinozoisite. Whereas the compressibility of the *a*-axis is nearly the same for both phases, the *b*- and *c*-axes of the epidote are about 1.5 times more compressible than in clinozoisite, consistent with epidote having a lower bulk modulus. Raman spectra collected up to 40.4 GPa also show no indication of phase transformation and were used to obtain mode Grüneisen parameters (γ_i) for Si–O vibrations, which were found to

be 0.5–0.8, typical for hydrous silicate minerals. The average pressure coefficient of Raman frequency shifts for M–O modes in epidote, $2.61(6) \text{ cm}^{-1}/\text{GPa}$, is larger than found for clinozoisite, $2.40(6) \text{ cm}^{-1}/\text{GPa}$, mainly due to the different compressibility of FeO₆ and AlO₆ octahedra in M3 sites. Epidote and clinozoisite contain about 2 wt% H₂O are thus potentially important carriers of water in subducted slabs.

Keywords Epidote · Clinozoisite · Synchrotron single-crystal X-ray diffraction · Compressibility

Introduction

Epidote-group minerals are common hydrothermal alteration minerals in basaltic rocks and potentially important carriers of H₂O in subducted oceanic crust. Epidote is also a common secondary mineral in marbles and schists and occurs as a pervasive replacement in geothermal systems experiencing multiple stages of epidote formation and dissolution (Bird and Spieler 2004). Monoclinic epidote-group minerals along the join between epidote [end member: Ca₂Al₂(Fe³⁺)(SiO₄)(Si₂O₇)O(OH)] and clinozoisite [end member: Ca₂Al₃(SiO₄)(Si₂O₇)O(OH)] are typically associated with low-grade metamorphism and hydrothermal activity at 250–400 °C and 1–2 kbars. Poli and Schmidt (1998, 2004) showed that epidote and clinozoisite are stable over a wide pressure and temperature range in both continental and ocean crust in continental collisions and subduction zones (Enami et al. 2004). The composition of epidote is variable, with Fe³⁺ content (i.e., mol fraction of epidote end member) depending on bulk rock and fluid composition (Bird and Spieler 2004; Shikazono 1984). Monoclinic epidote with less than 50 % mol fraction of the

✉ Xiang Wu
xiang.wu@pku.edu.cn

¹ Key Laboratory of Orogenic Belts and Crustal Evolution, MOE, Peking University and School of Earth and Space Sciences, Peking University, Beijing 100871, China

² Key Laboratory of High Temperature and High Pressure Study of the Earth's Interior, Institute of Geochemistry, Guiyang 550081, China

³ Shanghai Synchrotron Radiation Facility, Shanghai Institute of Applied Physics, Chinese Academy of Sciences, Shanghai 201204, China

⁴ Department of Earth and Planetary Sciences, Northwestern University, Evanston, IL 60208, USA

epidote end member is referred to as clinozoisite (Franz and Liebscher 2004). Through substitution, epidote-group minerals may also contain significant Mn_2O_3 , Cr_2O_3 , SrO , and rare earth elements.

Epidote-group phase equilibria reflect pressure–temperature conditions in geological processes. Monoclinic epidote, including clinozoisite, occurs in high- and ultra-high-pressure metamorphic rocks from a wide variety of geological settings. The structures of epidote and clinozoisite are similar, representing a class of monoclinic sorosilicates with both isolated SiO_4 tetrahedra and Si_2O_7 groups, combined with two distinct edge-sharing octahedral chains that run along the [010] direction. The octahedral sites are mainly occupied by Al and Fe^{3+} , and there is an extensive solid solution between clinozoisite and epidote (Franz and Liebscher 2004).

Several studies have shown the stability of epidote and clinozoisite is influenced not only by pressure and temperature, but also by the Al/ Fe^{3+} ratio, solution pH, fluid composition and oxygen fugacity (Bird and Spieler 2004; Bonazzi and Menchetti 1995; Holdaway 1972; Klemm 2004). Many previous studies have investigated the crystal chemistry and crystal structure of epidote-group minerals (Bonazzi and Menchetti 2004; Franz and Liebscher 2004; Gottschalk 2004). From previous compressibility experiments, there is a wide range in the reported values of the isothermal bulk modulus (K_{T0}) and first pressure derivative $K'_0 = (\text{d}K/\text{d}P)_{P=0}$ of epidote and clinozoisite. Holland et al. (1996) and Pawley et al. (1996) studied the compressibility of epidote and clinozoisite up to 8.2 GPa, reporting a $K_{T0} = 162(4)$ GPa for Fe-bearing epidote and 154(6) GPa for Fe-free clinozoisite. The P – V – T equation of state of epidote containing 0.745 Fe_{tot} pfu and 2.265 Al pfu was determined by Gatta et al. (2011) using synchrotron powder X-ray diffraction up to ~10 GPa and 1200 K, finding $K_{T0} = 111(3)$ GPa and $K'_0 = 7.6(7)$. Brillouin-scattering measurements on Fe-free, single-crystal zoisite by Mao et al. (2007) reported 125.3(4) GPa for the adiabatic bulk modulus (K_{S0}). The isothermal bulk modulus of single-crystal clinozoisite containing 0.22 Fe_{tot} pfu and 2.78 Al pfu was determined experimentally in static compression experiments with $K_{T0} = 127(5)$ GPa and $K'_0 = 0.5(2)$ (Comodi and Zanazzi 1997), whereas Fan et al. (2011) reported a value of bulk modulus of natural Fe-bearing clinozoisite containing about 0.1 Fe_{tot} pfu and 2.9 Al pfu with $K_{T0} = 138(3)$ GPa, fixing $K'_0 = 4$. There is a discrepancy between previous results of K_{T0} and K'_0 for natural epidote and clinozoisite minerals, possibly due to compositional differences but also experimental factors such as the number of data points, pressure range, and the choice of pressure medium.

Al \leftrightarrow Fe $^{3+}$ substitution along the clinozoisite-epidote join affects the crystal structure and crystal chemistry of

epidote-group minerals. In addition, the concentration and valence state of iron in silicates are known to influence elastic properties, with important implications for geophysical and geochemical studies of mineral properties at high pressures and temperatures. The natural occurrence and relatively high P – T stability fields of some hydrous minerals suggest that they are carriers of H_2O in the Earth's interior and are likely involved in metamorphic and melting reactions between the crust and upper mantle. Knowledge of the stability and thermoelastic properties of hydrous minerals such as epidote-group minerals is therefore relevant to understanding geological processes transferring volatiles between the Earth's crust and mantle. Here, we determine the compressibility and vibrational properties of natural epidote and clinozoisite by synchrotron-based, X-ray diffraction up to 30 GPa and Raman spectroscopy up to 40 GPa using single-crystal samples at room temperature. Although the diffraction data were collected in wide-scan mode and therefore not analyzed for intensity (structure refinements), the use of single-crystal samples allowed for both epidote and clinozoisite samples to be compressed in the same diamond-anvil cell experiment without peak overlap. The results are applied to determining the comparative compressibility of two natural epidote-group minerals and evaluating the effect of composition in the solid solution on compression behavior.

Experiment methods

A natural clinozoisite, gray-green in color from Pakistan, was chosen for high-pressure diffraction and Raman experiments. A natural, dark-green epidote sample used in this study was collected from Yunshan, Yunnan province in China. The chemical composition of the epidote and clinozoisite crystals was determined to be $\text{Ca}_{1.85}\text{Fe}_{0.79}\text{Al}_{2.19}\text{Ti}_{0.05}\text{Si}_{3.03}\text{O}_{12}(\text{OH})$ and $\text{Ca}_{1.97}\text{Fe}_{0.40}\text{Al}_{2.66}\text{Ti}_{0.03}\text{Si}_{3.03}\text{O}_{12}(\text{OH})$, respectively, based on electron microprobe analysis (EMPA) using a JEOL JXA-8230 electron microprobe with an accelerating voltage of 15 kV and a beam current of 20 nA. The ambient P – T unit-cell parameters, determined by synchrotron single-crystal X-ray diffraction at the beamline 15U of Shanghai Synchrotron Radiation Facility (SSRF), are $a = 8.9511(8)$ Å, $b = 5.6025(9)$ Å, $c = 10.195(2)$ Å, $\beta = 115.602(6)^\circ$ for epidote, and $a = 8.9109(8)$ Å, $b = 5.589(7)$ Å, $c = 10.276(1)$ Å, $\beta = 116.55(2)^\circ$ for clinozoisite, in good agreement with those obtained for samples of similar composition reported by Gatta et al. (2011) with $a = 8.8900(3)$ Å, $b = 5.6287(2)$ Å, $c = 10.1558(4)$ Å, and $\beta = 115.412(2)^\circ$ for epidote, and Fan et al. (2011) $a = 8.926(5)$ Å, $b = 5.629(7)$ Å, $c = 10.197(6)$ Å, and $\beta = 116.1(1)^\circ$ for clinozoisite, respectively. Single-crystal

samples were double-side polished into plates measuring about 10–15 microns in thickness using diamond lapping films.

A short symmetric-type diamond anvil cell (DAC) with 300- μm -diameter culets was used for both high-pressure X-ray diffraction and Raman spectroscopic experiments. The sample chamber was formed by drilling a 150- μm -diameter hole in a rhenium gasket that had been pre-indented to ~ 40 μm thickness. The polished epidote and clinozoisite samples were loaded into the sample chamber along with a small ruby sphere for pressure calibration according to the R1 fluorescence peak position (Mao et al. 1986). To achieve quasi-hydrostatic conditions and maintain similar pressure environments surrounding every crystal, we loaded the cells with neon as the pressure-transmitting medium for both X-ray diffraction and Raman spectroscopic experiments using the COMPRES/GSECARS gas-loading system (Rivers et al. 2008). The initial pressure inside the cell was about 2.5 GPa after gas loading. Reported pressure uncertainties reflect the difference between pressure measurements performed before and after each data collection, which did not vary by more than ± 0.2 GPa.

High-pressure synchrotron X-ray diffraction experiments were carried out at beamline 15U of SSRF. The wavelength of the monochromatic synchrotron radiation X-ray beam was $\lambda = 0.6199$ \AA and beam size = 3×4 μm^2 . XRD patterns from the single crystals were recorded using a rayonix SX165 CCD detector, calibrated with a CeO_2 standard using the program Fit2D (Hammersley et al. 1996). At each pressure, the DAC was continuously rotated from -20° to 20° about the X-ray beam direction with an exposure time of 10 s for every pattern. Diffraction data were collected in about 1 GPa steps on compression to 29.3 GPa. Peak positions and indexing of both samples (epidote and clinozoisite) were assigned using the GSE_ADA/RSV software package (Dera 2007). Unit-cell parameters were refined by least-squares fitting techniques using the UNITCELL (Holland and Redfern 1997) At least 22 reflections for each sample were used to refine the unit-cell parameters. In order to maintain consistency, only the peaks appearing at all pressure steps were included for high-pressure lattice parameter refinements.

High-pressure Raman spectroscopy was performed up to 40.4 GPa at room temperature in the Mineral Physics Laboratory, University of Texas at Austin. The Raman system uses a 532-nm Coherent Verdi V2 excitation laser. Neutral density filters were used to limit the power to ~ 50 mW at the sample to avoid excessive heating or damage to the sample. Spectra were collected with an electron multiplying charge-coupled device (EMCCD) and Andor Shamrock spectrometer. Each Raman spectrum was collected with a total exposure time of ~ 120 s. Spectra were collected in

unpolarized, backscatter geometry. Raman peak positions were fitted using the software package PeakFit (Systat Software, Inc.).

Results

X-ray diffraction

Single-crystal diffraction patterns taken at 2.5 and 29.4 GPa in wide-scan mode are shown in Fig. 1. Reflections from epidote and clinozoisite crystals appear as sharp, round spots in the patterns. No phase transition was observed for either epidote or clinozoisite over this pressure range.

The refined lattice parameters of epidote and clinozoisite at various pressures are listed in Table 1. The volume-compression data for epidote and clinozoisite are shown in Fig. 2. We first performed a second-order Birch–Murnaghan equation of state (BM2-EoS) fit to the P – V data using error-weighted least squares with EoSFit7c (Angel et al. 2014). Results of the BM2-EoS ($K'_0 = 4$ implied) yield the following results: $V_0 = 461.1(1)$ \AA^3 and $K_0 = 112.2(4)$ GPa for epidote; $V_0 = 457.8(1)$ \AA^3 and $K_0 = 153(1)$ GPa for clinozoisite. We applied the Fisher–Snedecor F test (Bevington and Robinson 2003) to our P – V data, finding that a third-order Birch–Murnaghan (BM3) fit provides a statistically better fit to both epidote and clinozoisite datasets at the 95 % confidence level ($p < 0.05$), where p is the false-rejection probability. The resulting BM3-EoS parameters are as follows: $V_0 = 461.1(1)$ \AA^3 , $K_0 = 115(2)$ GPa, and $K'_0 = 3.7(2)$ for epidote; $V_0 = 457.8(1)$ \AA^3 , $K_0 = 142(3)$ GPa, and $K'_0 = 5.2(4)$ for clinozoisite. Correlation between fitted EoS parameters K_0 and K'_0 was analyzed for both datasets and presented in Fig. 3.

Axial compression data of epidote and clinozoisite are plotted in Fig. 4, normalized to room pressure values. To determine the axial compressibility of a , b , and c in epidote and clinozoisite, we used a linearized BM2 fitting where in each axial dimension is cubed and treated as volume in the BM formulation (Angel et al. 2014). The zero-pressure axial compressibility of linear dimension l , defined as $\beta_{l0} = -(l^{-1})(\delta l/\delta P)_{P=0}$, is related to the linear modulus (linear incompressibility) by $M_{l0} = (\beta_{l0})^{-1}$. For epidote, our fitted linear moduli to a , b , and c are 313(4), 373(3), and 325(3) GPa, respectively, corresponding to axial compressibility values of $\beta_a = 3.19(4) \times 10^{-3}$, $\beta_b = 2.68(2) \times 10^{-3}$, and $\beta_c = 3.08(3) \times 10^{-3}$ GPa^{-1} . For clinozoisite, we obtain linear moduli for a -, b -, and c -axes of 320(2), 580(9), and 491(11) GPa, respectively, corresponding to axial compressibility values of $\beta_a = 3.13(2) \times 10^{-3}$, $\beta_b = 1.72(3) \times 10^{-3}$, and $\beta_c = 2.04(5) \times 10^{-3}$ GPa^{-1} . In both epidote and clinozoisite, there is considerable anisotropy in axial

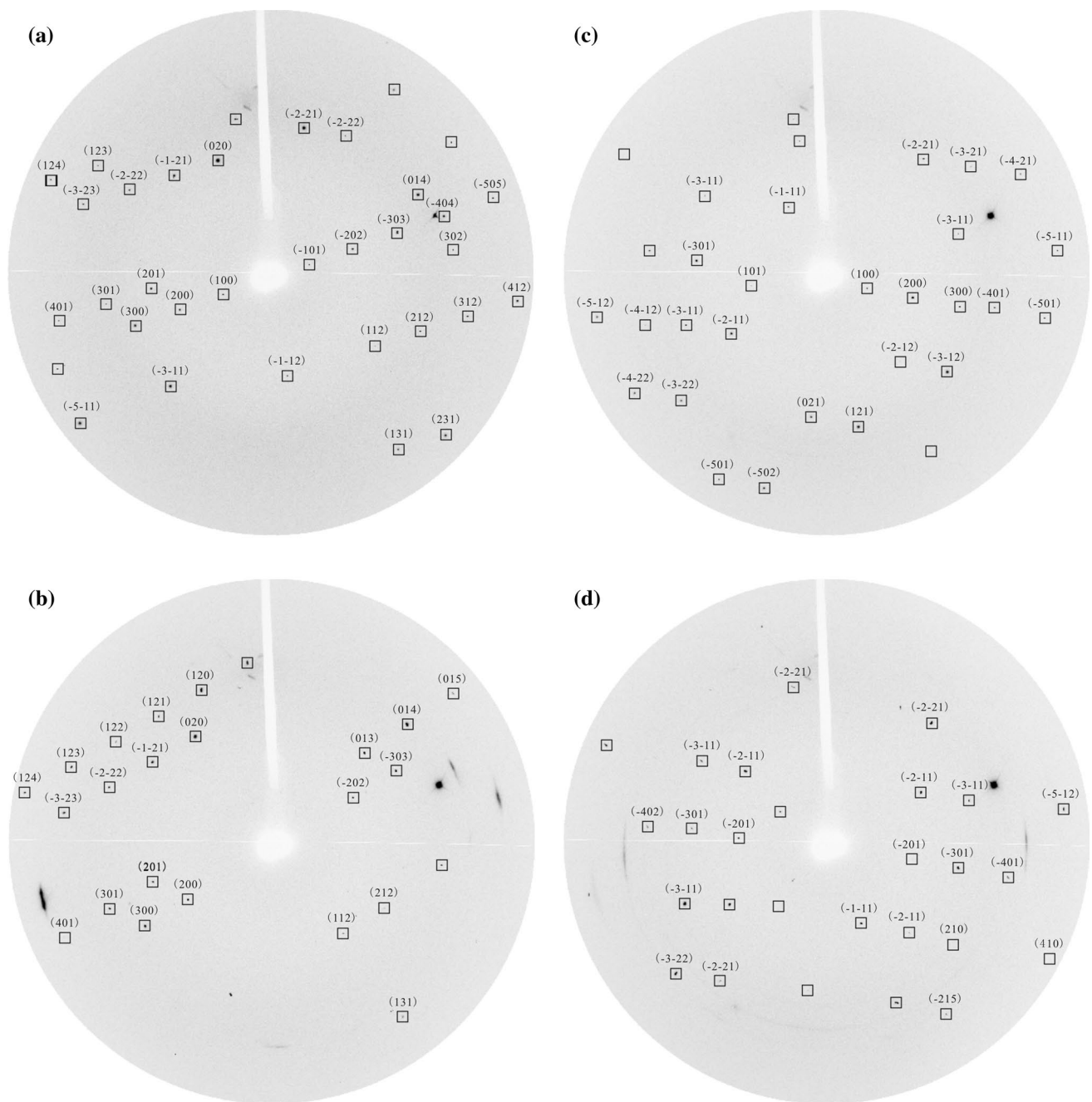


Fig. 1 Wide-scan diffraction patterns of single-crystal epidote (**a**, **b**) and clinozoisite (**c**, **d**) at 2.5 GPa (**a**, **c**) and 29.4 GPa (**b**, **d**) in the same diamond anvil cell. Indexed reflections are bound by boxes,

while the unmarked but very strong reflections are from the diamond anvils. Reflections due to crystalline neon are identified as streaks in **b** and **d**

compressibility, with the *b*-axis being the stiffest direction in both phases. The ratios of zero-pressure axial compressibility in epidote are 1.19:1.00:1.15, and for clinozoisite we find 1.82:1.00:1.19. Whereas the *a*-axis has nearly the same compressibility in both phases, the *b*- and *c*-axes of epidote are 1.5 times more compressible than in clinozoisite. The monoclinic β angle decreases continuously on compression within the pressure range. These relationships

are consistent with clinozoisite having a higher bulk modulus than epidote.

Raman spectroscopy

Raman spectra were conducted up to ~40 GPa on crystals taken from the same bulk samples of epidote and clinozoisite used in the diffraction study. We observed about 20

Table 1 Variation of lattice parameters with pressures for epidote and clinozoisite

<i>P</i> (GPa)	<i>a</i> (Å)	<i>b</i> (Å)	<i>c</i> (Å)	β (°)	<i>V</i> (Å ³)
<i>Epidote</i>					
0.0001	8.9511(7)	5.6025(8)	10.195(2)	115.602(5)	461.08(5)
2.5 ^a	8.8802(8)	5.5622(9)	10.119(2)	115.647(6)	450.57(7)
3.1	8.8729(8)	5.5535(9)	10.102(1)	115.708(5)	448.50(6)
3.7	8.8568(9)	5.543(1)	10.093(2)	115.675(7)	446.57(8)
4.4	8.8324(9)	5.533(1)	10.073(2)	115.624(7)	443.60(7)
6.6	8.8067(8)	5.513(1)	10.000(2)	115.624(7)	437.80(7)
7.4	8.7867(8)	5.504(1)	9.982(2)	115.680(6)	435.09(6)
8.8	8.7699(7)	5.490(9)	9.967(2)	115.74(6)	432.25(7)
9.7	8.7380(8)	5.4741(9)	9.949(1)	115.711(6)	428.80(6)
10.5	8.7140(8)	5.468(1)	9.914(1)	115.671(6)	425.77(6)
11.6	8.6957(8)	5.450(1)	9.903(2)	115.665(6)	423.01(6)
12.7	8.6742(2)	5.4415(9)	9.870(2)	115.713(6)	419.74(6)
13.7	8.6518(8)	5.428(1)	9.861(2)	115.699(6)	417.28(6)
14.7	8.6366(8)	5.427(1)	9.845(2)	115.706(6)	415.83(5)
15.8	8.6201(7)	5.4197(8)	9.809(2)	115.710(6)	412.88(5)
16.7	8.5923(9)	5.4028(9)	9.798(2)	115.658(6)	410.01(6)
17.7	8.5715(9)	5.3863(9)	9.778(2)	115.671(7)	406.87(6)
19.0	8.5560(8)	5.3769(9)	9.750(2)	115.680(6)	404.27(6)
20.5	8.5315(8)	5.3665(9)	9.738(2)	115.665(6)	401.86(6)
21.7	8.5191(9)	5.3581(9)	9.703(2)	115.737(6)	398.96(6)
22.7	8.5003(8)	5.3544(9)	9.680(2)	115.647(7)	397.16(5)
23.7	8.4752(8)	5.3475(9)	9.679(2)	115.646(7)	395.53(5)
24.7	8.4399(8)	5.3371(9)	9.660(2)	115.568(7)	392.53(5)
26.9	8.4172(7)	5.3163(9)	9.625(2)	115.565(7)	388.89(5)
28.0	8.4099(8)	5.3014(9)	9.592(2)	115.617(7)	385.59(6)
29.3	8.3837(8)	5.2953(9)	9.568(2)	115.522(7)	384.43(5)
<i>Clinozoisite</i>					
0.0001	8.9109(6)	5.589(1)	10.276(1)	116.552(1)	457.80(8)
2.5 ^a	8.8530(7)	5.5739(7)	10.246(1)	116.56(1)	452.24(9)
3.1	8.8427(7)	5.5715(7)	10.241(1)	116.68(2)	450.80(9)
3.7	8.8127(6)	5.5592(1)	10.230(1)	116.56(2)	448.30(9)
4.4	8.7988(7)	5.545(1)	10.209(1)	116.67(2)	445.2(1)
5.4	8.7774(6)	5.5366(7)	10.192(1)	116.80(1)	442.09(8)
6.6	8.7534(6)	5.5266(7)	10.164(1)	116.71(2)	439.72(8)
7.4	8.7356(5)	5.5213(7)	10.140(1)	116.42(1)	437.49(8)
8.8	8.7058(6)	5.5122(7)	10.117(1)	116.44(2)	434.70(9)
9.7	8.6822(6)	5.5034(7)	10.102(1)	116.55(1)	431.79(9)
10.5	8.6616(5)	5.4978(7)	10.082(1)	116.18(2)	430.34(8)
11.6	8.6396(5)	5.4872(7)	10.057(1)	116.38(1)	427.11(8)
12.7	8.6191(6)	5.4790(7)	10.044(1)	116.51(2)	424.46(9)
13.7	8.5992(5)	5.4722(7)	10.024(1)	116.35(1)	422.70(8)
14.7	8.5875(5)	5.4661(7)	10.016(1)	116.29(1)	421.50(8)
15.8	8.5609(5)	5.4570(7)	9.989(1)	116.11(1)	419.96(8)
16.7	8.5457(6)	5.4455(1)	9.987(1)	115.86(2)	417.68(8)
17.7	8.5273(6)	5.4418(7)	9.977(1)	115.94(2)	416.11(8)
19.0	8.5136(6)	5.4294(9)	9.959(1)	116.21(2)	413.04(9)
20.5	8.4810(6)	5.4251(9)	9.932(1)	116.53(2)	410.02(8)

Table 1 continued

<i>P</i> (GPa)	<i>a</i> (Å)	<i>b</i> (Å)	<i>c</i> (Å)	β (°)	<i>V</i> (Å ³)
21.7	8.4788(6)	5.4158(9)	9.927(1)	116.40(2)	407.89(8)
22.7	8.4717(6)	5.4119(9)	9.920(1)	116.40(2)	406.28(8)
23.7	8.4602(7)	5.4052(9)	9.904(1)	116.31(2)	405.28(8)
24.7	8.4286(6)	5.3974(9)	9.891(1)	116.21(2)	403.72(9)
26.9	8.4101(6)	5.3923(1)	9.862(1)	116.22(2)	401.24(8)
28.0	8.3834(6)	5.3864(9)	9.860(1)	116.15(3)	399.67(8)
29.3	8.3714(8)	5.3783(9)	9.840(1)	116.01(2)	398.17(9)

^a Nominal uncertainty in pressure is ± 0.2 GPa

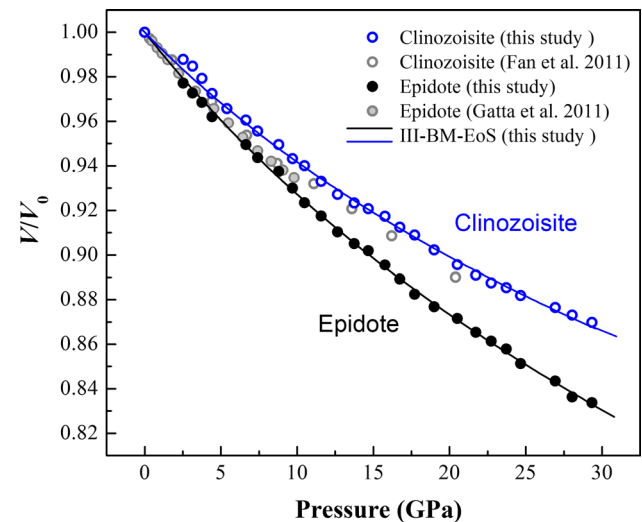


Fig. 2 Volume–pressure data for epidote and clinozoisite from the current and previous studies. Third-order Birch–Murnaghan fits to the volume compression from this study are shown by the *solid* curves

vibrational mode frequencies (ν_i), compared with group theory calculations of 57 Raman-active modes for epidote and 60 for clinozoisite (Aroyo et al. 2006a, b). The smaller number of observed modes is due to weak intensity, peak overlap, and orientation dependence. Selected Raman spectra of epidote and clinozoisite loaded together in the same diamond cell at high pressures are plotted together in Fig. 5. The room pressure spectra of both phases are similar to those from previous studies (Liebscher 2004) and reference spectra from the University of Arizona RRUFF database (Lafuente et al. 2015) #R048809 and #R040085, shown in Fig. 5 for comparison. All Raman modes show a continuous shift to higher frequency with increasing pressure. No peaks merge and no new peaks appear over the experimental pressure range, consistent with the X-ray diffraction data indicating structural stability of both phases at room temperature up to 40 GPa.

Raman spectra of epidote and clinozoisite are similar in the region between 200 and 1200 cm^{-1} on compression. At

Fig. 3 Confidence ellipses for EoS parameters fitted to the data for epidote (a), and clinozoisite (b), at the 68.3 % (darker) and 95.4 % (lighter) confidence limits

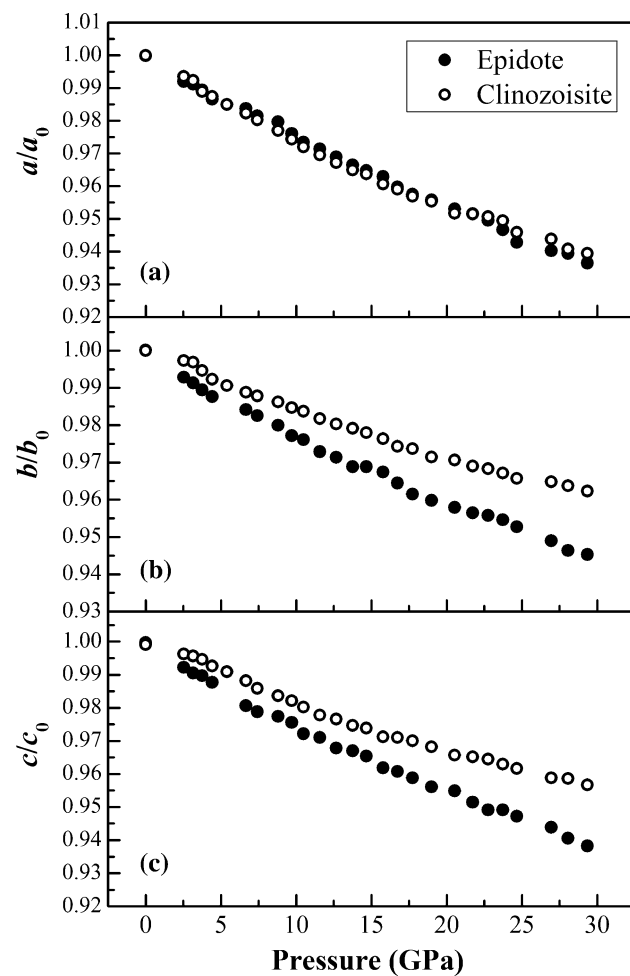
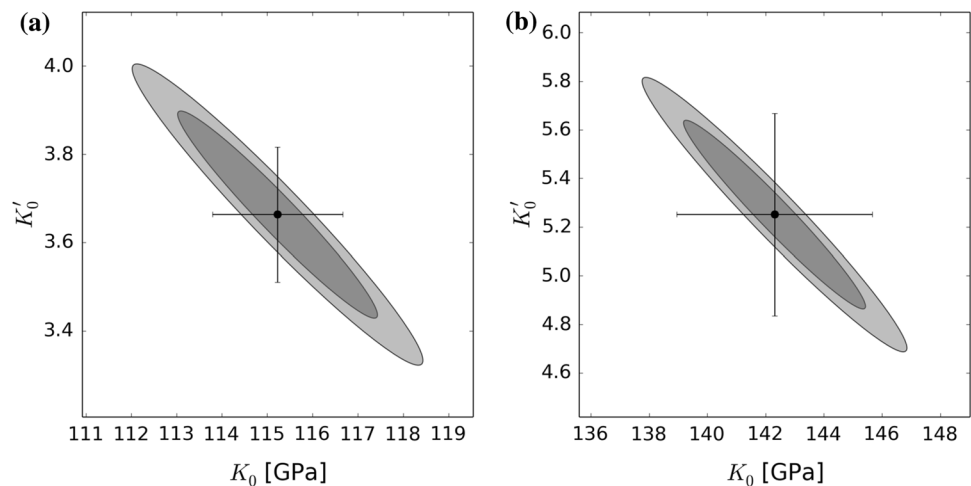


Fig. 4 Pressure dependence of normalized unit-cell parameters, a/a_0 , b/b_0 and c/c_0

320–540 cm^{-1} , four modes are observed in both samples mainly from M–O vibrations (M = Al and/or Fe in epidote) within the different octahedral chains (epidote: 359,

396, 461, and 508 cm^{-1} ; clinozoisite: 359, 398, 462, and 515 cm^{-1}). The Raman shift at 284 cm^{-1} of epidote and 286 cm^{-1} of clinozoisite may be associated with the Ca–O vibration as inferred from studies of zoisite and clinozoisite (Langer and Raith 1974). Mode frequencies in the 450–750 and 800–1100 cm^{-1} ranges empirically arise from symmetric stretching Si–O vibrations (Wang et al. 1994). We therefore assigned the strong band pair at 572 and 606 cm^{-1} in epidote, and at 577 and 610 cm^{-1} in clinozoisite, to Si–O. In addition, Raman bands at 841, 893, and 975 cm^{-1} in epidote, and 843, 892 and 971 cm^{-1} in clinozoisite, are also attributed to Si–O vibrations in SiO_4 and Si_2O_7 groups (Bradbury and Williams 2003). For both samples, the strong band at approximately 435 cm^{-1} can be attributed to the Si–O–Si bending.

Figure 6 illustrates the pressure dependence of Raman mode frequencies. The assignment of Raman modes follows the notation of Langer and Raith (1974) and Makreski et al. (2007). All results are summarized in Table 2. Mode frequencies were fitted linearly by $\omega_i = \omega_{i0} + \alpha_i \times P$, where ω_{i0} is the frequency of mode i at 0 GPa, α_i is the linear pressure coefficient $(\partial\omega_i/\partial P)_{P=0}$, and P is the pressure. The mode Grüneisen parameters (γ_i) are calculated by $\gamma_{i0} = -\partial(\ln\omega_i)/\partial(\ln V) = (K_{T0}/\omega_{i0})\alpha_i$ (Born and Huang, 1954). We used the bulk modulus $K_{T0} = 115(2)$ GPa for epidote and $K_{T0} = 142(3)$ GPa for clinozoisite, which were obtained by the BM3 fit, to calculate the mean γ_i values. The resulting values of Ca–O vibrations are 0.81(2) for epidote and 1.25(4) for clinozoisite. For the Si–O-related vibrations, the calculated γ_i values range from 0.5 to 0.8 with average γ values of 0.53(1) and 0.67(3) for epidote and clinozoisite, respectively.

Discussion

Both epidote and clinozoisite in space group $P2_1/m$ are sorosilicates having an additional isolated SiO_4 tetrahedron

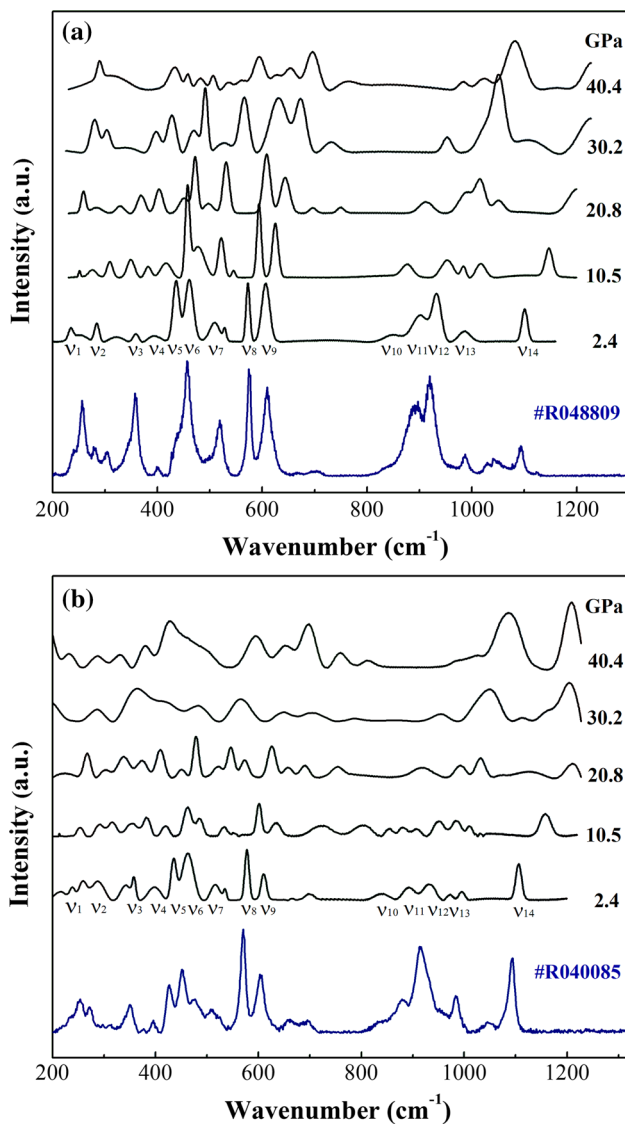


Fig. 5 Selected Raman spectra of epidote (a) and clinozoisite (b) at various pressures. Raman spectra from the RRUFF database (Lafuente et al. 2015) for epidote (#R048809) and clinozoisite (#R040085) are also shown for comparison

in the general formula, $A_1A_2M_1M_2M_3(\text{SiO}_4)(\text{Si}_2\text{O}_7)\text{O}(\text{OH})$. M cations in octahedral site with coordination number (CN) = 6 are mainly occupied by Al and Fe^{3+} , and the A cations with CN > 6 are mainly occupied by Ca. The structure is built up by two edge-sharing octahedral chains running parallel to the *b*-axis with three non-equivalent M1, M2, and M3 octahedra; a single chain of M2 and a zig-zag chain of M1 with M3-polyhedra attached on the alternate sides along its length (Franz and Liebscher 2004). Among M1O_6 , M2O_6 , and M3O_6 octahedra, M3O_6 is the largest and most distorted, while M2O_6 is the smallest and the least distorted (Nagashima 2011). The two distinct octahedral chains are bridged in [100] and [001] directions

by isolated single SiO_4 and Si_2O_7 tetrahedral groups. As in clinozoisite, the substitution of Fe^{3+} for Al involves the M3 sites, which is different in size and shape from the octahedral chain sites M1 and M2.

Referring to Table 3, the bulk modulus obtained here for epidote of 115(2) GPa from the BM3 fit is in good agreement with 111(3) GPa obtained by Gatta et al. (2011) and 116(7) GPa reported by Fan et al. (2014). For clinozoisite, our bulk modulus of 142(3) GPa is statistically higher than 127(4) GPa reported by Comodi and Zanazzi (1997) and 138(3) GPa obtained by Fan et al. (2011). There is generally lack of agreement in the first pressure derivative K'_0 . Whereas we found $K'_0 = 3.7(2)$ and $5.2(4)$ for epidote and clinozoisite, respectively, the fitted value of K'_0 for epidote was 7.6(7) from Gatta et al. (2011) and 7.8(8) from Fan et al. (2014). For clinozoisite, Comodi and Zanazzi (1997) obtained $K'_0 = 0.5(2)$ but only fitted to data over a very limited pressure range of 5.1 GPa. The reason for these discrepancies is not immediately clear, but because our data cover a wider pressure range (30 GPa) with around 1 GPa steps, the current dataset may offer improved constraints on K'_0 . Fitting the *P*–*V* data in XRD compression experiments suffers from a well-known negative correlation between K_0 and K'_0 , illustrated in Fig. 3. The difference between the derived pressure derivatives of the bulk modulus obtained in this study and those reported in previous studies may likely due to: the limited *P*-range investigated, i.e., ~5.2 GPa in Holland et al. (1996), ~9.8 GPa in Gatta et al. (2011), the different pressure media (Table 3), and also possibly the different Fe contents, although the $\text{Fe}_{\text{tot}} = 0.79$ pfu in epidote from this study is very similar to $\text{Fe}_{\text{tot}} = 0.745$ pfu from the study of Gatta et al. (2011). However, since the epidote and clinozoisite were compressed in the same diamond cell in this study, the comparative values of K'_0 between epidote and clinozoisite should be considered robust.

Our results on the compressibility of epidote and clinozoisite can also be compared with other sorosilicates in the epidote group, e.g., Fe-free zoisite $K_{T0} = 122.1(7)$ GPa and Fe-rich zoisite $K_{T0} = 119.1(7)$ GPa (Alvaro et al. 2012) as well as lawsonite $K_0 = 125(2)$ GPa (Grevet et al. 2000), and K_{T0} (or adiabatic K_{S0}) values in some related studies are ranging from 102(6.5) to 136(4) GPa (Comodi and Zanazzi 1997; Mao et al. 2007; Pawley et al. 1998; Sinogeikin et al. 2000; Winkler et al. 2001), which are still in a reasonable agreement. Comparing the two compositions in this study, the $\text{Fe}_{\text{tot}} = 0.79$ pfu in epidote is about twice that in clinozoisite with $\text{Fe}_{\text{tot}} = 0.40$ pfu, and owing to the fact that Fe^{3+} has ~14 % larger ionic radius than that of Al^{3+} (CN = 6, Fe^{3+} : 0.785 Å and Al^{3+} : 0.675 Å), the iron content likely plays a role. Increasing Fe content generally reduces O–O repulsion by increasing the M3 octahedral dimensions, while the other M1 and M2 polyhedral

Fig. 6 Pressure dependence of observed vibrational frequency modes (ν_i) from Raman spectroscopy for epidote (a) and clinozoisite (b). Solid lines were obtained using linear regressions, provided in Table 2

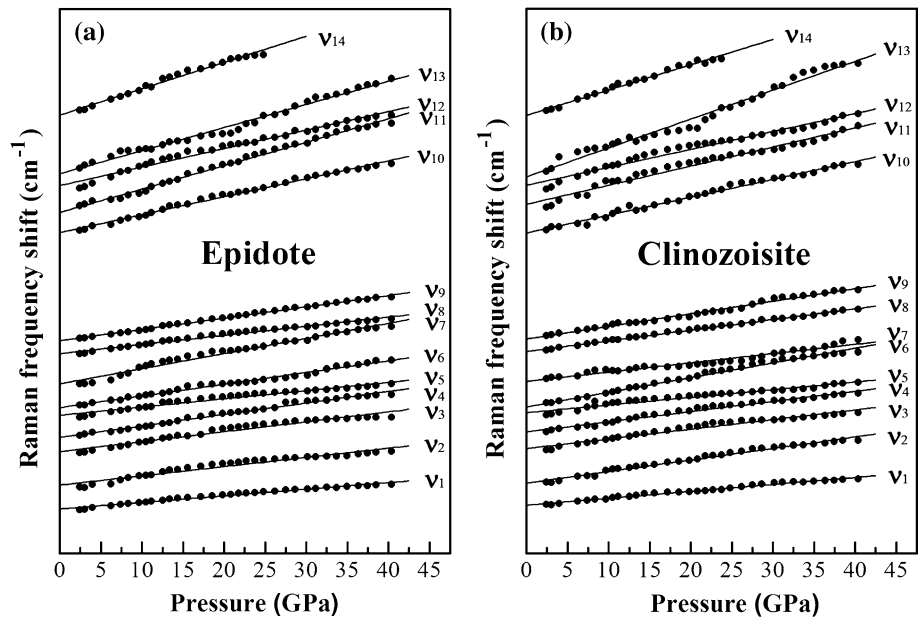


Table 2 Results of linear regressions to the pressure dependence of observed vibrational modes (ν_i) in epidote and clinozoisite up to 40 GPa

Epidote				Clinozoisite				Assignment
Modes	ω_0 (cm ⁻¹)	α (cm ⁻¹ /GPa)	γ_i	Modes	ω_0 (cm ⁻¹)	α (cm ⁻¹ /GPa)	γ_i	
ν_1	234	1.43(4)	0.70(2)	ν_1	236	1.52(3)	0.91(3)	
ν_2	285	2.00(9)	0.81(2)	ν_2	286	2.52(6)	1.25(4)	Ca–O
ν_3	361	2.15(8)	0.69(2)	ν_3	361	2.12(7)	0.83(3)	M–O
ν_4	392	2.49(5)	0.73(2)	ν_4	398	2.23(6)	0.80(3)	M–O
ν_5	435	1.80(7)	0.48(1)	ν_5	440	1.69(6)	0.55(2)	Si–O
ν_6	456	2.53(5)	0.64(2)	ν_6	453	3.23(7)	1.01(2)	M–O
ν_7	507	3.28(7)	0.74(2)	ν_7	509	2.04(5)	0.57(2)	M–O
ν_8	573	1.97(4)	0.40(1)	ν_8	575	2.33(2)	0.58(2)	Si–O
ν_9	601	2.45(2)	0.47(1)	ν_9	602	2.77(5)	0.65(2)	Si–O
ν_{10}	835	3.91(6)	0.54(1)	ν_{10}	836	3.93(7)	0.67(2)	Si–O
ν_{11}	879	5.07(7)	0.66(2)	ν_{11}	899	4.20(12)	0.66(2)	Si–O
ν_{12}	937	4.00(10)	0.49(1)	ν_{12}	940	3.95(11)	0.60(2)	Si–O
ν_{13}	963	5.02(10)	0.60(1)	ν_{13}	960	6.35(16)	0.94(3)	Si–O
ν_{14}	1089	5.70(16)	0.60(2)	ν_{14}	1095	5.57(15)	0.72(3)	Si–O

The reference frequency at room pressure (ω_0) and pressure coefficients, $\alpha_i = (d\omega_i/dP)$, were used to calculate mode Grüneisen parameters (γ_i) using the fitted K_{T0} values obtained in this study from BM3-EoS fits: 115(2) GPa for epidote and 142(3) GPa for clinozoisite

volumes remain practically constant (Comodi and Zanazzi 1997). The increase in volume of M3 is accommodated by increasing the distance between the cation and the apical O atoms. Furthermore, an increase in Fe content in epidote may facilitate the rotation of SiO₄ tetrahedra (Alvaro et al. 2012).

To investigate the compression anisotropy of epidote and clinozoisite, we fitted the linear compressibility (β_0) along each axis using the BM2 formulation in EoSFit7c (Angel et al., 2014). In both phases, the *b*-axis was found to be the least compressible, which might be expected for the

direction containing more SiO₄ tetrahedra or Si₂O₇ groups per unit length than other directions. The zero-pressure β ratios ($\beta_a:\beta_b:\beta_c$) for epidote are 1.19:1.00:1.15, and for the clinozoisite we found 1.82:1.00:1.19. In both phases, we find $\beta_a > \beta_c > \beta_b$, and thus the largest anisotropy in compressibility is between the *a*- and *b*-axes. Comparing the two compositions, epidote and clinozoisite possess nearly the same linear compressibility in the *a*-axis direction, but both *b*- and *c*-axes of epidote with about twice as much Fe are ~1.5 times more compressible than in clinozoisite (Fig. 4). According to our results, the higher Fe content in

Table 3 Summary of compressibility studies of epidote and clinozoisite

Mineral	References	Fe _{tot} pfu	P _{max} /(GPa)	K ₀ /(GPa)	K' ₀	Pressure medium ^a	Method
Epidote	This study	0.79	29.4	115(2)	3.7(2)	Neon	XRD(SC)
	This study	0.79	29.4	112.2(4)	4 (fixed)	Neon	XRD(SC)
	Holland et al. (1996)	0.96	5.21	162(4)	4 (fixed)	ME = 4:1	XRD(PD)
	Gatta et al. (2011)	0.745	9.80	111(3)	7.6(7)	ME = 4:1	XRD(PD)
	Fan et al. (2014)	0.5	9.16	116(7)	7.8(8)	MEW = 16:3:1	XRD(PD)
Clinozoisite	This study	0.4	29.4	142(3)	5.2(4)	Neon	XRD(SC)
	This study	0.4	29.4	153(1)	4 (fixed)	Neon	XRD(SC)
	Holland et al. (1996)	0.02	8.20	154(6)	4 (fixed)	ME = 4:1	XRD(PD)
	Comodi and Zanazzi (1997)	0.22	5.1	127(4)	0.5(2)	MEW = 16:3:1	XRD(SC)
	Fan et al. (2011)	0.1	20.4	138(3)	4 (fixed)	MEW = 16:3:1	XRD(PD)
	Winkler et al. (2001)	0	50	136(4)			DFT

SC single crystal, PD powder diffraction, DFT density function theory

^a ME = 4:1, 4:1 methanol–ethanol mixture; MEW = 16:3:1, 16:3:1 methanol–ethanol–water mixture

epidote leads to a significant increase in the linear compressibility of the *b*- and *c*-axes compared with clinozoisite. For epidote with Fe_{tot} = 0.745 pfu, Gatta et al. (2011) also found the *b*-axis to be the least compressible; however, in that study, which used a linearized BM3 fit, the *a*-axis was less compressible than *c*, giving linear compressibility ratios $\beta_a:\beta_b:\beta_c$ of 1.08:1.00:1.40. In contrast, Alvaro et al. (2012) reported that in zoisite the *a*-axis is the least compressible, with linear axial compressibility ratios of 1.00:2.31:2.74 for Fe-free zoisite and 1.00: 2.34:2.99 for zoisite with Fe_{tot} = 0.12 pfu. Clearly, further studies are required to more fully understand the effects of Fe content and structure on the axial compressibility of epidote-group minerals.

Raman spectroscopy is a sensitive technique to probe the characteristics of cation–anion coordination groups. The pressure coefficients, $\alpha_i = (d\omega_i/dP)_{P=0}$, give quantitative comparisons for the changes of different vibration modes with pressure (Table 2). Raman modes are assigned by comparing our results with previous ambient pressure data (Makreski et al. 2007; Bradbury and Williams 2003; Langer and Raith 1974). The pressure coefficient of Ca–O bond in epidote is somewhat different than that in clinozoisite, which is partly attributed to the different energy of bands. As for the silicate-derived vibration in both phases, the calculated γ values fall generally in the range of 0.5–0.8, which are typical for some hydrous silicates, e.g., phase D and phase E. By comparing with dense hydrous magnesium silicates, the internal Si–O modes of phase E possess the nearly same range in γ values, 0.53–0.83 (Shieh et al. 2009). The calculated mode Grüneisen parameters for epidote and clinozoisite in this study are ranging from 0.40(1) to 0.81(2) (epidote) and 0.55(2)–1.25(4) (clinozoisite), with average values from all the observed modes of 0.61(1) and 0.77(3), respectively.

The mean pressure coefficient of M–O modes in epidote of 2.61(6) cm⁻¹/GPa is slightly larger than 2.40(6) cm⁻¹/GPa found in clinozoisite, consistent with the higher compressibility of epidote relative to clinozoisite. The pressure coefficient of Si–O modes in epidote, 3.74 cm⁻¹/GPa, is nearly the same with in uncertainty to 3.85 cm⁻¹/GPa for clinozoisite. We therefore conclude that the major difference in compressibility between the two structures is related to M–O bonds and in particular FeO₆ and AlO₆ octahedra in M3 sites. Our conclusion that the addition of Fe into epidote reduces its bulk modulus is consistent with the findings of Gatta et al. (2011).

Epidote-group minerals are commonly found in a wide range of crustal rocks and hydrothermally altered basalt. At 600–700 °C, a breakdown of epidote-group minerals is typically observed, but they can be stabilized to higher temperatures by incorporation of rare earth elements (Hermann 2002). The combined influence of temperature and pressure on clinozoisite can be evaluated by the volume-expansion-to-compression-ratio about 38 bar/K (Comodi and Zanazzi 1997), indicating that the thermal behavior of epidote-group minerals remains stable along the geothermal gradient. As potential carriers of H₂O into the upper mantle, the physical properties of epidote-group minerals at simultaneous high pressures and temperatures warrant further investigation of their elastic properties to assist in calculations of predicted seismic wave speeds in hydrated slabs.

Conclusion

The comparative compressibility of a natural epidote (Fe_{tot} = 0.79) and clinozoisite (Fe_{tot} = 0.40) was examined by loading both crystals simultaneously into the same diamond-anvil cell experiment up to 30 GPa. The results show

that increasing iron content reduces the bulk modulus and increases the first pressure derivative (K'_0) in the BM3-EoS formulation. In combination with Raman spectroscopy performed up to 40 GPa, we find no evidence for phase transformation over this pressure range at 300 K. We found the *b*-axis to be the least compressible, and the addition of Fe appears to significantly increase the linear compressibility of the *b*- and *c*-axes of epidote, leading to an overall reduction in bulk modulus of epidote compared with clinozoisite. We attribute the differences in compression behavior to the addition of Fe at M3 site in the epidote structure. Raman spectra further suggest that the difference in compressibility between epidote and clinozoisite is likely due to the different compressibility of FeO_6 and AlO_6 octahedra in M3 sites.

Acknowledgments This research was supported by the National Natural Science Foundation of China (U1232204 and 41473056) and in part through a scholarship to FQ by the Chinese Scholarship Council. SDJ acknowledges support from the US National Science Foundation through grant EAR-1452344 and the David and Lucile Packard Foundation. Use of the COMPRES/GSECARS gas-loading system was supported by COMPRES under NSF Cooperative Agreement No. EAR 11-57758 and by GSECARS through NSF Grant No. EAR-1128799 and DOE Grant No. DE-FG02-94ER14466. Portions of this work were performed at the Mineral Physics Laboratory of the University of Texas at Austin, and we would like to thank J.F. Lin for help with Raman spectroscopy.

References

- Alvaro M, Angel RJ, Camara F (2012) High-pressure behavior of zoisite. *Am Mineral* 97:1165–1176
- Angel RJ, Alvaro M, Gonzales-Platas J (2014) EosFit7c and a Fortran module (library) for equation of state calculations. *Z Kristallogr* 229:405–419
- Aroyo MI, Perez-Mato JM, Capillas C, Kroumova E, Ivantchev S, Madariaga G, Kirov A, Wondratschek H (2006a) Bilbao crystallographic server: I. Databases and crystallographic computing programs. *Z Kristallogr* 221:15–27
- Aroyo MI, Kirov A, Capillas C, Perez-Mato JM, Wondratschek H (2006b) Bilbao crystallographic server. II. Representations of crystallographic point groups and space groups. *Acta Cryst A* 62:115–128
- Bevington PR, Robinson DK (2003) Data reduction and error analysis for the physical sciences, 3rd edn. McGraw-Hill, New York
- Bird DK, Spieler AR (2004) Epidote in geothermal systems. *Rev Miner Geochem* 56:235–300
- Bonazzi P, Menchetti S (1995) Monoclinic members of the epidote group: effects of the $\text{Al} \leftrightarrow \text{Fe}^{3+} \leftrightarrow \text{Fe}^{2+}$ substitution and of the entry of REE^{3+} . *Miner Mag* 53:133–153
- Bonazzi P, Menchetti S (2004) Manganese in monoclinic members of the epidote group: piemontite and related minerals. *Rev Miner Geochem* 56:495–552
- Born M, Huang K (1954) Dynamical theory of crystal lattices. Oxford University Press, UK
- Bradbury SE, Williams Q (2003) Contrasting bonding behavior of two hydroxyl-bearing metamorphic minerals under pressure: Clinozoisite and topaz. *Am Miner* 88:1460–1470
- Comodi P, Zanazzi PF (1997) The pressure behavior of clinozoisite and zoisite: an X-ray diffraction study. *Am Miner* 82:61–68
- Dera P (2007) GSE-ADA data analysis program for monochromatic single crystal diffraction with area detector. GeoSoilEnviro-CARS, Argonne, Illinois
- Enami M, Mizukami T, Yokoyama K (2004) Metamorphic evolution of garnet-bearing ultramafic rocks from the Gongen area, Sanbagawa belt, Japan. *J Metamorph Geol* 22:1–15
- Fan DW, Ma MN, Yang JJ, Wei SY, Chen ZQ, Xie HS (2011) In situ high-pressure synchrotron X-ray diffraction study of clinozoisite. *Chin Phys Lett* 28:126103
- Fan DW, Xu JG, Wei SY, Chen ZQ, Xie HS (2014) In situ high-pressure synchrotron X-ray diffraction of natural epidote. *Chin J High Press Phys* 28:257–261 (in Chinese)
- Franz G, Liebscher A (2004) Physical and chemical properties of the epidote minerals: an introduction. *Rev Miner Geochem* 56:1–82
- Gatta GD, Merlini M, Lee Y, Poli S (2011) Behavior of epidote at high pressure and high temperature: a powder diffraction study up to 10 GPa and 1200 K. *Phys Chem Miner* 38:419–428
- Gottschalk M (2004) Thermodynamic properties of zoisite, clinozoisite and epidote. *Rev Miner Geochem* 56:83–124
- Grevel KD, Nowlan EU, Fasshauer DW, Burchard M (2000) In situ X-ray diffraction investigation of lawsonite and zoisite at high pressures and temperatures. *Am Miner* 85:206–216
- Hammersley AP, Svensson SO, Hanfland M, Fitch AN, Hausermann D (1996) Two-dimensional detector software: from real detector to idealised image or two-theta scan. *High Pres Res* 14:235–248
- Hermann J (2002) Allanite: thorium and light rare earth element carrier in subducted crust. *Chem Geol* 192:289–306
- Holdaway MJ (1972) Thermal stability of Al-Fe epidote as a function of $f\text{O}_2$ and Fe content. *Contrib Min Pet* 37:307–340
- Holland TJB, Redfern SAT (1997) Unit cell refinement from powder diffraction data: the use of regression diagnostics. *Miner Mag* 61:65–77
- Holland TJB, Redfern SAT, Pawley AR (1996) Volume behavior of hydrous minerals at high pressure and temperature: II. Compressibilities of lawsonite, zoisite, clinozoisite, and epidote. *Am Miner* 81:341–348
- Klemm R (2004) Fluid inclusions in epidote minerals and fluid development in epidote-bearing rocks. *Rev Miner Geochem* 56:197–234
- Lafuente B, Downs RT, Yang H, Stone N (2015) The power of databases: the RRUFF project. In: Armbruster T, Danisi RM (eds) Highlights in mineralogical crystallography. W. De Gruyter, Berlin, pp 1–30
- Langer K, Raith M (1974) Infrared spectra of Al-Fe(III)-epidotes and zoisites, $\text{Ca}_2(\text{Al}_{1-p}\text{Fe}^{3+}_p)\text{Al}_2\text{O}(\text{OH})[(\text{Si}_2\text{O}_7)[\text{SiO}_4]]$. *Am Miner* 59:1249–1258
- Liebscher A (2004) Spectroscopy of epidote minerals. *Rev Miner Geochem* 56:125–170
- Makreski P, Jovanovski G, Kaitner B, Gajović A, Biljan T (2007) Minerals from Macedonia XVIII. Vibrational spectra of some sorosilicates. *Vib Spectrosc* 44:162–170
- Mao HK, Xu J, Bell P (1986) Calibration of the ruby pressure gauge to 800 kbar under quasi-hydrostatic conditions. *J Geophys Res* 91:4673–4676
- Mao Z, Jiang FM, Duffy TS (2007) Single-crystal elasticity of zoisite $\text{Ca}_2\text{Al}_3\text{Si}_3\text{O}_{12}(\text{OH})$ by Brillouin scattering. *Am Miner* 92:570–576
- Nagashima M (2011) Pumpellyite-, sursassite-, and epidote-type structures: common principles-individual features. *J Miner Pet Sci* 106:211–222
- Pawley AR, Redfern SAT, Holland TJB (1996) Volume behavior of hydrous minerals at high pressure and temperature: I. Thermal expansion of lawsonite, zoisite, clinozoisite, and diasporite. *Am Miner* 81:335–340

- Pawley AR, Chinnery NJ, Clark SM (1998) Volume measurements of zoisite at simultaneously elevated pressure and temperature. *Am Miner* 83:1030–1036
- Poli S, Schmidt MW (1998) The high-pressure stability of zoisite and phase relationships of zoisite-bearing assemblages. *Contrib Miner Pet* 130:162–175
- Poli S, Schmidt MW (2004) Experimental subsolidus studies on epidote minerals. *Rev Miner Geochem* 56:171–195
- Rivers M, Prakapenka VB, Kubo A, Pullins C, Holl CM, Jacobsen SD (2008) The COMPRES/GSECARS gas-loading system for diamond anvil cells at the Advanced Photon Source. *High Pres Res* 28:273–292
- Shieh SR, Duffy TS, Liu ZX, Ohtani E (2009) High-pressure infrared spectroscopy of the dense hydrous magnesium silicates phase D and phase E. *Phys Earth Planet Inter* 175:106–114
- Shikazono N (1984) Compositional variations in epidote from geothermal areas. *Geotherm J* 18:181–187
- Sinogeikin SV, Schilling FR, Bass JD (2000) Single crystal elasticity of lawsonite. *Am Miner* 85:1834–1837
- Wang A, Han J, Guo L, Yu J, Zeng P (1994) Database of standard Raman spectra of minerals and related inorganic crystals. *Appl Spectrosc* 48:959–968
- Winkler B, Milman V, Nobes RH (2001) A theoretical investigation of the relative stabilities of Fe-free clinozoisite and ortho­zoisite. *Phys Chem Miner* 28:471–474